AIP | Physics of Fluids

Capillary effects on floating cylindrical particles

Harish N. Dixit and G. M. Homsy

Citation: Physics of Fluids (1994-present) **24**, 122102 (2012); doi: 10.1063/1.4769758
View online: http://dx.doi.org/10.1063/1.4769758
View Table of Contents: http://scitation.aip.org/content/aip/journal/pof2/24/12?ver=pdfcov
Published by the AIP Publishing

PHYSICS OF FLUIDS **24**, 122102 (2012)

Capillary effects on floating cylindrical particles

Harish N. Dixit[a] and G. M. Homsy[b]
Department of Mathematics, University of British Columbia, Vancouver, British Columbia V6T 1Z4, Canada

(Received 11 September 2012; accepted 17 November 2012; published online 7 December 2012)

In this study, we develop a systematic perturbation procedure in the small parameter, $B^{1/2}$, where B is the Bond number, to study capillary effects on small cylindrical particles at interfaces. Such a framework allows us to address many problems involving particles on flat and curved interfaces. In particular, we address four specific problems: (i) capillary attraction between cylinders on flat interface, in which we recover the classical approximate result of Nicolson ["The interaction between floating particles," Proc. Cambridge Philos. Soc. **45**, 288–295 (1949)], thus putting it on a rational basis; (ii) capillary attraction and aggregation for an infinite array of cylinders arranged on a periodic lattice, where we show that the resulting Gibbs elasticity obtained for an array can be significantly larger than the two cylinder case; (iii) capillary force on a cylinder floating on an arbitrary curved interface, where we show that in the absence of gravity, the cylinder experiences a lateral force which is proportional to the gradient of curvature; and (iv) capillary attraction between two cylinders floating on an arbitrary curved interface. The present perturbation procedure does not require any restrictions on the nature of curvature of the background interface and can be extended to other geometries. © *2012 American Institute of Physics*. [http://dx.doi.org/10.1063/1.4769758]

I. INTRODUCTION

Capillary attraction between floating particles is a phenomenon of everyday experience that causes the particles at fluid interfaces to aggregate.[1] This is sometimes called the "Cheerios effect"[2] because of the tendency for a popular breakfast cereal to aggregate on the interface. Particulate aggregates at an interface can occur for a wide range of particle sizes, ranging from the nanometer range[3] to millimeter sized particles.[4–10] At the heart of capillary attraction is the interfacial deformation caused by a balance of surface tension and the net weight of the particles,[11] which is usually relevant for particles larger than a few micrometers and is also the focus of the present study.

In addition to the problems addressed in this paper, particles at interfaces are of general interest. For sub-micrometer particles,[12] microscopic forces like the long-range van der Waals forces can lead to attraction and electrostatic forces to repulsion, and the particles themselves are subject to Brownian motion. Since the work of Ramsden[13] and Pickering[14] it is well known that solid particles on interfaces can be used effectively as a stabilizing agent in emulsions.[15,16] The contact angle made by particles at an interface is thought to be a measure of the hydrophile-lipophile balance. But unlike surfactants, the energy required to desorb a particle from an interface is very high, often requiring energies many orders of magnitude larger than thermal energy k_BT,[16,17] making them excellent emulsifiers. The affinity of particles to an interface together with strong lateral attractions between them has been exploited in recent years to create novel structures called "colloidosomes," solid capsules made of micrometer-size solid particles.[18] In addition, solid particles have also been used to create "colloidal armour," a protective covering on drops and bubbles;[19] 2D crystals in

[a]Electronic mail: hdixit@math.ubc.ca.
[b]Electronic mail: bud@math.ubc.ca.

an evaporating thin film;[20] and non-spherical bubbles[21] due to jamming of the particles. In many of the above applications, gravitational forces are negligible due to small size of the particles. At high concentration of particles, an interface acquires elasticity and can be described as a composite layer.[22] The Young's modulus of such an interface has been measured recently for non-Brownian particles.[23] It has been suggested that particles at an interface can have similarities with surfactants.[17] The analogy has been extended further in recent times with measurements of surface tension as a function of particle concentration.[22,24–26] This has led to empirical modeling of the equation of state of such composite layers,[27] similar in spirit to the Gibbs equation[28] for surfactant-laden interfaces describing the variation of surface tension as a function of surfactant concentration. The key point which makes particle-laden interfaces so important in technological applications is the presence of cohesive interaction between the particles. In this study, we restrict ourselves to situations where gravity alone is important and hence neglect other interaction forces.

The first detailed study of capillary interaction between spherical bubbles at a liquid-gas interface is due to Nicolson.[29] In Nicolson's calculation, the interface deformation due to a single bubble is first calculated. The energy of interaction is then calculated by placing a second bubble at a given distance and assuming that the interface shape is the same as that for a single bubble. This procedure is therefore akin to a pairwise additive assumption and is referred to as the Nicolson approximation or the linear superposition approximation. Because of its simplicity, the Nicolson approximation is regularly used in studies involving capillary attraction. On the other hand, Gifford and Scriven[30] obtained numerical solutions to the full nonlinear problem of capillary attraction between cylinders without approximation and found that at small Bond numbers, the force-distance relationship is well described by an exponential function. This result was subsequently reconciled by Chan *et al.*[31] who extended the Nicolson approximation to solid cylindrical and spherical particles and showed that the force of attraction between floating cylinders evaluated using the Nicolson approximation also decreases exponentially with distance. Like many approximations, the range of applicability of the Nicolson approximation is unknown and difficult to establish. Allain and Cloitre[32] used a free energy analysis to study the interaction between two horizontal cylinders. Because of the complexity of the resulting equations, they resorted to numerical methods and showed that the Nicolson approximation should be valid in an asymptotic regime at small Bond numbers. Other approximations for capillary attraction between particles have also been developed. Kralchevsky *et al.*,[33] using the solution of the linearized Young-Laplace equation in bipolar coordinates, calculated the force of attraction between two spheres resting on a solid surface wetted by a liquid. Paunov *et al.*[34] extended this methodology for freely floating spherical particles on an interface. A detailed survey of many key results in particle-laden interfaces is contained in the excellent monograph of Kralchevsky and Nagayama.[10]

Most of the approaches highlighted in the previous paragraph fall under the general category of "energy-based" approaches in which the free energy of interaction is first calculated and is then used to obtain the force of attraction. There exist a few works that have used a force-based approach in which the solution of the Young-Laplace equation is used directly to calculate the capillary force of attraction. The most prominent of these is the aforementioned paper by Gifford and Scriven, which was the first work to use this approach to calculate attraction between two horizontal cylinders. Allain and Cloitre[35] derived the Nicolson approximation with a force-based approach by obtaining the interface shape by solving a linearized Young-Laplace equation due to a single cylinder. An important contribution was made by Vassileva *et al.*[8] who used a series solution in Bessel functions to calculate capillary attractions between multiple particles. The Nicolson approximation emerges as the leading term in their solution procedure. They also consider the effect of background curvature on the capillary attraction using another series expansion. Though Vassileva *et al.* follow a general approach with spherical particles on an interface, the coefficients of their series expansion have to be calculated numerically which becomes quite cumbersome. In this work, we look for asymptotic solutions to the Young-Laplace equation with a small Bond number, which differs from the approach of Vassileva *et al.*[8] A summary of the above studies shows that there is no rigorous asymptotic derivation of the Nicolson approximation in the small Bond number regime. In addition, none of the studies consider the case of multi-particle interactions in an analytically tractable way; most of the available studies with multiple particles use a simple vector addition of the Nicolson formula.

The present work is motivated from experiments on dip-coating flow[36] with surface adsorbed particles. The experiments revealed that with the addition of particles, film thickening was observed, resulting in positive deviations from the Landau-Levich law.[37,38] Hydrodynamic theories for surfactant effects on the Landau-Levich problem have been developed which predict film thickening[39–41] which have also been verified experimentally.[42,43] Similar hydrodynamic approaches can be developed for particle effects on the Landau-Levich problem. A crucial aspect for such models is the stress boundary condition at the interface and the form it takes in the presence of particles. This will require a detailed understanding of the interaction between particles at the interface and the forces that result.

In the case of a single particle floating on a curved interface, there are very few works dealing with the lateral force on the particle due to curvature effects. Kralchevsky *et al.*[44] use the method of images to calculate the force on a spherical particle on a curved interface near a wall. In the absence of gravity, Würger[45] considered the problem of a sphere on a curved interface, but his analysis is valid for interfaces with zero mean curvature. He found that the lateral force on a particle is proportional to the gradient of curvature, a result we obtain in our 2D calculation. Kralchevsky *et al.*[46] numerically studied interaction between particles residing on a spherical drop in bipolar coordinates. Though this analysis is valid for an interface with mean curvature, it is limited to a spherical geometry. Even in the absence of gravity, two particles can experience lateral attractive forces if the contact line is undulating. Stamou *et al.*[47] showed the existence of long range attractive forces in such cases and these attractions can be understood as due to the interactions between capillary quadrupoles or multipoles.[48] Such interactions due to undulating contact lines are beyond the scope of this paper. In fact, the approach of Danov and Kralchevsky[48] can also be applied to understanding interactions between particles in the presence of gravity.

In this paper, we develop an asymptotic method for computing capillary attraction in the limit of small Bond number for particles floating on flat and curved interfaces. For simplicity, we restrict our calculations to floating cylinders, but the approach is generalizable to 3D. We consider only non-Brownian particles, and therefore the relevant forces are gravity and surface tension. To the best of our knowledge, such an asymptotic approach has not been developed before. Since the Nicolson approximation is expected to give acceptable results at small Bond number, our first objective is to establish this approximation using systematic perturbation techniques. Since an isolated pair of particles is rarely encountered in reality as particles tend to aggregate into clusters, obtaining the capillary attraction force for an array of particles and analyzing its stability forms our second objective. Finally, particles at curved interfaces tend to climb up menisci. Observations on meniscus-climbing insects[49] have been explained using unbalanced capillary forces due to curved menisci. Cavallaro *et al.*[50] used curvature gradients to move rod-like particles to create self-assemblies. Motivated by these experiments, we apply our approach to the case of an interface with a mean curvature. These issues are most easily pursued for the case of aligned cylinders, but the approach and the insight gained carry over to more complicated situations, most practically to that of spheres.

The outline of the paper is as follows. In Sec. II, we first formulate the governing force balance equations for solid particles at an interface. In Sec. III, we calculate the force of attraction between two parallel cylinders on an initially flat interface. The general framework of our asymptotic approach is also outlined in this section. We then study the case of an array of cylinders on a flat interface in Sec. IV. This result is useful to understand aggregation for large number of particles. In Sec. V, we extend our asymptotic approach to the case of a floating cylinder on an arbitrary curved interface. The case of capillary attraction between two cylinders on a curved interface is given in Sec. VI. Section VII summarizes our results and discusses the implications of the results obtained in the present paper to related problems.

II. FORMULATION

Consider a static configuration of two horizontal cylinders of infinite length and radius R, density ρ_s floating on an interface between two fluids of densities ρ_A and ρ_B with $\rho_B > \rho_A$, and separated by a center-to-center distance, d, as shown in Figure 1. Our formulation is similar to that given in

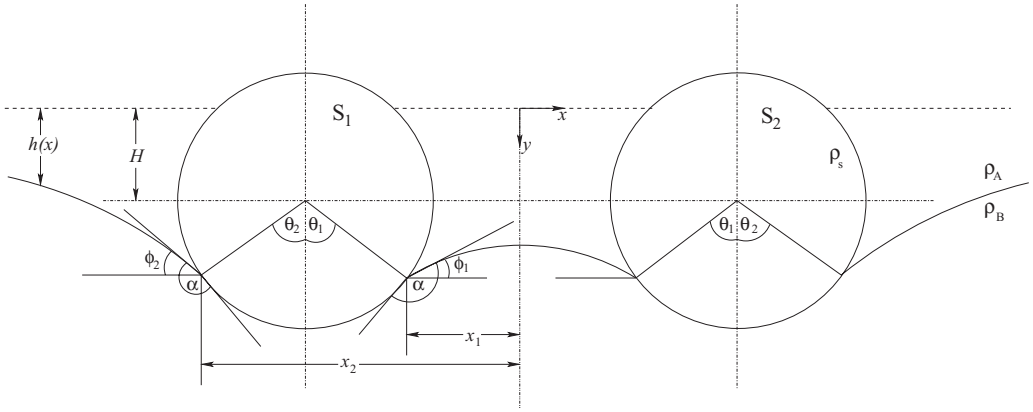

FIG. 1. Parallel cylinders of equal radius R separated by a center-to-center distance d floating at an interface separating fluids A and B.

Gifford and Scriven.[30] Later in the paper, this configuration will be suitably modified to account for background curvature effects and for the case of an array of cylinders. The contact angle, $\alpha \in [0, \pi]$, measured in the lower fluid is the same on either side of each cylinder and is taken to be fixed[51] at its equilibrium value, but the position of the contact line is allowed to vary with varying separation distance between the particles. Far from the cylinders the interface is flat and is taken to be the plane of zero pressure. The depth to which the cylinders sink[52] below this level is denoted by H, θ_1 and θ_2 are the wetting angles subtended by the contact line measured from the vertical, and $\phi_i = (\alpha + \theta_i - \pi)$, $i = 1, 2$ is the angle made by the interface with the horizontal. Let F be the horizontal force of attraction between the cylinders per unit length of the cylinder, referred to below as simply "the force." We will show later that asymmetry in the meniscus shape around each cylinder results in a non-zero attractive force. For simplicity, we consider identical cylinders to demonstrate the analytical procedure. This leads to a symmetry plane midway between the two cylinders. Therefore, it is sufficient to analyze the force balance on a single cylinder with a symmetry condition replacing the boundary condition. Moreover, the present approach can be extended easily to account for cylinders of different radii or contact angles. The total pressure, in dimensional form, below the fluid interface is related to the atmospheric pressure, P_0, above the interface by the relation

$$p = P_0 + (\rho_B - \rho_A)gh + \sigma(\nabla \cdot \mathbf{n}), \tag{1}$$

where σ is the surface tension, $\mathbf{n}$ is the unit normal to the liquid pointing from fluid A to fluid B, and g is the acceleration due to gravity which acts in the y direction. Without loss of generality, P_0 can be taken to zero. The vertical force balance can be written as

$$F_w = -\mathbf{e_y} \cdot \int_{\Gamma_c+\Gamma_b} p\mathbf{n}dl = F_b + F_\sigma, \tag{2}$$

where F_w is the total weight of the cylinder per unit length, i.e., $F_w = \rho_s g\pi R^2$, Γ_c is the contour of integration taken along the fluid interface and Γ_b is the contour of integration taken along the surface of the particle. The buoyancy contribution is given by

$$F_b = \mathbf{e_y} \cdot \int_{\Gamma_b} (\rho_B - \rho_A)gh\mathbf{n}dl, \tag{3}$$

and the capillary pressure (curvature) contribution becomes

$$F_\sigma = \mathbf{e_y} \cdot \int_{\Gamma_c} \sigma(\nabla \cdot \mathbf{n})\mathbf{n}dl. \tag{4}$$

In the case of an arbitrarily shaped three-dimensional floating body, Keller[53] has shown that the vertical components of the curvature force, F_σ and the buoyancy force F_b are equal to the weight of the liquid displaced by the meniscus. For an isolated floating body, the net horizontal force then

vanishes. But in the presence of another floating body, the buoyancy and curvature forces result in an unbalanced horizontal force given by

$$F = \mathbf{e_x} \cdot \int_{\Gamma_c+\Gamma_b} p\mathbf{n}dl. \tag{5}$$

The above integrals can be evaluated in terms of the parameters shown in Figure 1.

In order to present certain geometric expressions in an economical way, we non-dimensionalize all length scales by the radius of the cylinder: non-dimensional variables are indicated with an asterisk and all forces are per unit axial length of the cylinder and are scaled by the surface tension. The relative contribution of buoyancy and curvature forces can be expressed in terms of the Bond number

$$B = \frac{g(\rho_B - \rho_A)R^2}{\sigma} = \frac{R^2}{l_c^2}, \tag{6}$$

where $l_c = \sqrt{\sigma/(\rho_B - \rho_A)g}$ is the capillary length. In terms of the parameters shown in Figure 1, vertical equilibrium for each cylinder is expressed by the following dimensionless equation:

$$B\left\{\theta_1 + \theta_2 + \frac{1}{2}\left[\sin(2\theta_1) + \sin(2\theta_2)\right] + 2H^*\left[\sin(\theta_1) + \sin(\theta_2)\right]\right\}$$
$$= 2\left[\sin(\alpha + \theta_1) + \sin(\alpha + \theta_2)\right] + 2\pi B D, \tag{7}$$

where $D = (\rho_s - \rho_A)/(\rho_B - \rho_A)$ is the density parameter, and $H^* = H/R$ is the non-dimensional height to which the cylinders are displaced vertically relative to a flat interface far from the cylinders. In Eq. (7), the term on the left hand side and first and second terms of the right hand side represent contributions from the buoyancy force, surface tension force, and the weight of the particle, respectively. Similarly, the horizontal force balance can be written in non-dimensional form as

$$F^* = \frac{F}{\sigma} = \left[\cos(\alpha + \theta_2) - \cos(\alpha + \theta_1)\right]$$
$$+B\left\{H^*(\cos(\theta_1) - \cos(\theta_2)) + \frac{1}{2}\left(\sin^2(\theta_2) - \sin^2(\theta_1)\right)\right\}. \tag{8}$$

In this equation, the first and second terms on the right hand side represent contributions from surface tension and buoyancy force, respectively. For particles with a small radius or when the gravitational force is weak relative to surface tension, the Bond number is small. In this limit, the vertical and horizontal force balances are dominated by the surface tension contribution. Notice that the horizontal force, F^*, vanishes when the interface shape is symmetric on either side of the cylinder, i.e., $\theta_1 = \theta_2$. Hence, an attractive force is created only in the presence of an asymmetry in the interface shape on either side of the cylinder. This is the basis of capillary attraction.

Equations (7) and (8) establish general relationships between F^*, H^*, θ_1, and θ_2. The last three of these are of course constrained by the conditions of interfacial equilibrium, subject to the contact angle conditions. The shape of the interface is governed by the Young-Laplace equation. This is obtained from Eq. (1) by equilibrating the hydrostatic pressure with the capillary pressure, and can be written in non-dimensional form as

$$\nabla \cdot \mathbf{n} = -Bh^*. \tag{9}$$

The above equations are identical to those of Gifford and Scriven[30] and were solved using a numerical technique. Here, we develop an asymptotic theory in the limit of small Bond number. In this limit, the slope of the interface is small, allowing linearization of the curvature about a flat undisturbed interface. Equation (9) becomes

$$\frac{d^2h^*}{dx^{*2}} = Bh^*. \tag{10}$$

The general solution of (10) is

$$h^*(x^*) = ae^{-B^{1/2}x^*} + be^{B^{1/2}x^*}, \tag{11}$$

where a, b are constants of integration to be determined by applying boundary conditions. The locations of the contact lines (x_1^* and x_2^* in Figure 1) are geometrically related to the separation distance d. Therefore, the force of attraction depends on four non-dimensional parameters - B, D, α and d^*, where $d^* = d/R$. From Eqs. (7) and (8), for every solution given by values (D, θ_1, θ_2, α), a complimentary solution ($1 - D$, $\pi - \theta_1$, $\pi - \theta_2$, $\pi - \alpha$) exists which is equivalent to flipping Figure 1 upside down.

The basic approach in this paper is to assume a configuration and first equilibrate the vertical force on a particle. We then calculate the shape of the interface due to all particles using Eq. (11) and the associated boundary conditions. Once H^*, θ_1, and θ_2 are known, the horizontal force of attraction is then calculated.

III. TWO CYLINDERS ON A FLAT INTERFACE

In this section, we obtain the force of attraction for two identical parallel cylinders on a horizontal interface for the geometry shown in Figure 1. This configuration has a symmetry plane midway between the two cylinders. In the present calculations, we calculate the force of attraction of the left cylinder, S_1. For convenience, the origin is chosen at the intersection of the undisturbed flat interface and the plane of symmetry. The boundary conditions for the interface between cylinders S_1 and S_2 are

$$\frac{dh^*}{dx^*} = 0, \quad \text{at} \quad x^* = 0, \tag{12}$$

$$\frac{dh^*}{dx^*} = -\tan(\phi_1), \quad \text{at} \quad x^* = -x_1^*. \tag{13}$$

The interface shape between the two cylinders is found to be

$$h^*(x^*) = B^{-1/2}\tan(\phi_1)\left[\frac{\cosh\left(B^{1/2}x^*\right)}{\sinh\left(B^{1/2}x_1^*\right)}\right], \qquad \forall -x_1^* \le x^* \le x_1^*. \tag{14}$$

Similarly, the boundary conditions on the interface to the left of cylinder S_1 are

$$\frac{dh^*}{dx^*} = 0, \quad \text{as} \quad x^* \to -\infty, \tag{15}$$

$$\frac{dh^*}{dx^*} = \tan(\phi_2), \quad \text{at} \quad x^* = -x_2^*, \tag{16}$$

and the interface shape to the left of cylinder S_1 becomes

$$h^*(x^*) = B^{-1/2}\tan(\phi_2)\exp\left(B^{1/2}\left(x^* + x_2^*\right)\right), \qquad \forall x^* \le -x_2^*. \tag{17}$$

The horizontal position of the contact line, x_1 and x_2 are geometrically related to the wetting angles by

$$x_1^* = \frac{d^*}{2} - \sin(\theta_1), \qquad x_2^* = \frac{d^*}{2} + \sin(\theta_2). \tag{18}$$

In addition, the vertical position of the contact line is geometrically related to the wetting angles through the solution of the Young-Laplace equation. At $x^* = -x_i^*$, $h^* = H^* + \cos(\theta_i)$ where $i = 1$, 2. This gives us two additional equations relating these geometric quantities

$$B^{1/2}\left[H^* + \cos(\theta_1)\right]\tanh(x_1^* B^{1/2}) = \tan(\phi_1), \tag{19}$$

$$B^{1/2}\left[H^* + \cos(\theta_2)\right] = \tan(\phi_2). \tag{20}$$

Equations (7) and (18)–(20) are the relevant governing transcendental equations involving the five unknowns (H^*, x_1^*, x_2^*, θ_1, θ_2). The nature of Eqs. (19) and (20) suggests that all the unknown quantities

may be expanded in simple powers of $B^{1/2}$ as follows:

$$H^* = \sum_{i=0}^{\infty} B^{i/2} H^{(i)}, \tag{21}$$

$$x_1^* = \sum_{i=0}^{\infty} B^{i/2} x_1^{(i)}, \tag{22}$$

$$x_2^* = \sum_{i=0}^{\infty} B^{i/2} x_2^{(i)}, \tag{23}$$

$$\theta_1^* = \sum_{i=0}^{\infty} B^{i/2} \theta_1^{(i)}, \tag{24}$$

$$\theta_2^* = \sum_{i=0}^{\infty} B^{i/2} \theta_2^{(i)}. \tag{25}$$

Since this is a simple regular perturbation, the leading order is identical to the case $B = 0$, which is equivalent to absence of gravity. Therefore, the solution is a flat interface with the vertical position of the particle determined such that the angle between the tangent to the cylinder and the interface is equal to the contact angle.[11,54] The leading order solution is therefore given by

$$H^{(0)} = \cos(\alpha), \qquad \theta_1^{(0)} = \theta_2^{(0)} = \pi - \alpha,$$
$$x_1^{(0)} = \frac{d^*}{2} - \sin(\alpha), \qquad x_2^{(0)} = \frac{d^*}{2} + \sin(\alpha). \tag{26}$$

In the expressions that follow, it is convenient to define the following secondary quantities:

$$\chi = \pi D - (\pi - \alpha) - \frac{1}{2}\sin(2\alpha), \tag{27}$$

$$S = \sin(\alpha), \quad C = \cos(\alpha). \tag{28}$$

The calculations can be pursued to a reasonably high order, but they are tedious and the details are omitted here. The results are given in Table I and have been verified with the symbolic software package MATHEMATICA. As discussed above, asymmetry in the interface shape is observed when $\theta_1 \neq \theta_2$. From Table I, we notice that the wetted angles θ_1 and θ_2 are equal at $\mathcal{O}(B^{1/2})$ and hence there is no force of attraction at this order. But the cylinders rise or fall due to their finite buoyancy, thus vertically distorting the interface. Asymmetry first appears at $\mathcal{O}(B)$ since $\theta_1^{(2)} \neq \theta_2^{(2)}$, creating the potential for capillary attraction. The expansion procedure was continued further to yield the solution up to $\mathcal{O}(B^3)$, which is not shown in the table due to its length. The resulting expression for force obtained from Eq. (8) reveals that the first non-zero contribution for force appears at $\mathcal{O}(B^2)$

TABLE I. Terms in expansions (21)–(25) for two isolated cylinders on a flat interface through $\mathcal{O}(B^2)$.

	θ_1	θ_2	x_1^*	x_2^*	H^*
B^0	$\pi - \alpha$	$\pi - \alpha$	$\frac{d^*}{2} - S$	$\frac{d^*}{2} - S$	C
$B^{1/2}$	0	0	0	0	χ
B^1	0	χ	0	$-\chi C$	$-\chi\frac{d^*}{2}$
$B^{3/2}$	$\left(\frac{d^*}{2} - S\right)\chi$	$-\left(\frac{d^*}{2} + S\right)\chi$	$\left(\frac{d^*}{2} - S\right)\chi C$	$\left(\frac{d^*}{2} + S\right)\chi C$	$\left(\frac{d^{*2}}{4} - S^2\right)\chi$
B^2	$-\frac{d^*}{2}\left(\frac{d^*}{2} - S\right)\chi$	$\frac{d^*}{2}\left(\frac{d^*}{2} + S\right)\chi$	$-\frac{d^*}{2}\left(\frac{d^*}{2} - S\right)\chi C$	$-\frac{\chi^2}{2}S - \frac{d^*}{2}\left(\frac{d^*}{2} + S\right)\chi C$	$\frac{\chi^2}{2}C + \frac{5\chi}{3}S^3 - \chi\frac{d^*}{3}\left(\frac{d^{*2}}{4} - \frac{3}{2}S^2\right)$

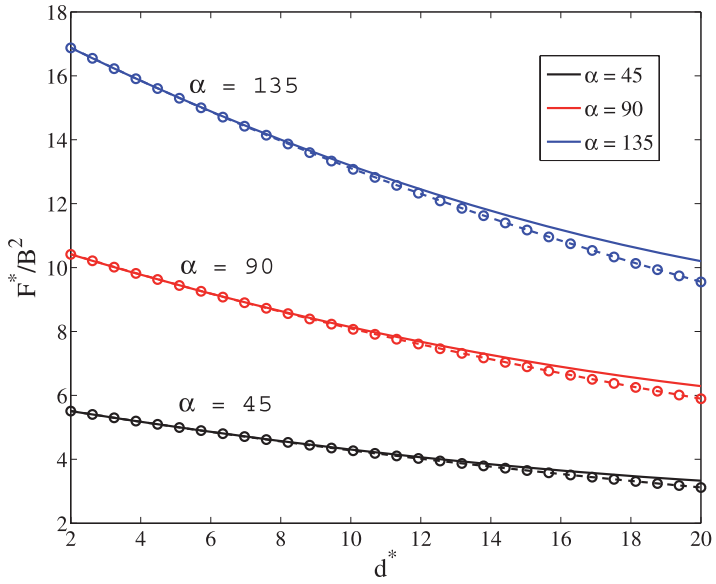

FIG. 2. Comparison between asymptotic results (solid line), the numerical solution (symbols) and the Nicolson approximation (dashed line) for three different contact angles. The density ratio is fixed at $D = 2$ and Bond number $B = 0.001$.

and can be written as

$$F_f^* = \frac{B^2\chi^2}{2}\left[1 - B^{1/2}d^* + B\left(\frac{d^{*2}}{2} - \sin^2(\alpha)\right)\right] + \mathcal{O}(B^{7/2}), \tag{29}$$

where the subscript f indicates that the undisturbed interface in the absence of particles is flat. To understand why lateral forces do not arise at $\mathcal{O}(B)$ even with the presence of an asymmetry, we write Eq. (8) as

$$F_f^* = F_\sigma^* + BF_b^*, \tag{30}$$

where F_σ^* and F_b^* represent curvature and buoyancy contributions as discussed earlier. Clearly, the dominant contribution to the lateral force arises from $F_\sigma^* = (\cos(\alpha + \theta_2) - \cos(\alpha + \theta_1))$. Using the leading order solution (26), the expansion for $\cos(\alpha + \theta_2)$ becomes

$$\cos(\alpha + \theta_2) = -1 + \frac{1}{2}B\theta_2^{(1)^2} + B^{3/2}\theta_2^{(1)}\theta_2^{(2)} + B^2\left\{-\frac{1}{24}\theta_2^{(1)^4} + \frac{1}{2}\left(\theta_2^{(2)^2} + 2\theta_2^{(1)}\theta_2^{(3)}\right)\right\} + \mathcal{O}(B^{5/2}). \tag{31}$$

Since $\theta_1^{(1)} = \theta_2^{(1)} = 0$, the leading term in F_σ^*, and hence F_f^* is $\mathcal{O}(B^2)$.

Chan *et al.*[31] and Allain and Cloitre[35] obtained the force of attraction between horizontal cylinders using the Nicolson approximation, which in the present variables can be written as

$$F_N^* = \frac{F_N}{\sigma} = \frac{B^2\chi^2}{2}e^{-B^{1/2}d^*}, \tag{32}$$

where the subscript N denotes the Nicolson approximation. Expanding the exponential terms in F_N^*, the leading terms in F_f^* (Eq. (29)) and F_N^* agree. We can thus see that leading terms of the Nicolson approximation appear naturally following the procedure outlined above and can be understood as an expansion in the small parameter $B^{1/2}d^*$. Note that the current asymptotic method avoids the usual superposition approximations. The only simplification made in the above analysis is the linearization of Young-Laplace equation. This is justified on two counts: first, the solutions are sought at small B where interface slope is small, and second, our main motivation is to derive Nicolson approximation rigorously which itself was obtained using linearization of curvature. The asymptotic expansion demonstrates that the deviation from the exponential form occurs at $\mathcal{O}(B^3)$. In Figure 2, we present a sample calculation comparing the present asymptotic solution (Eq. (29)) to numerical solutions

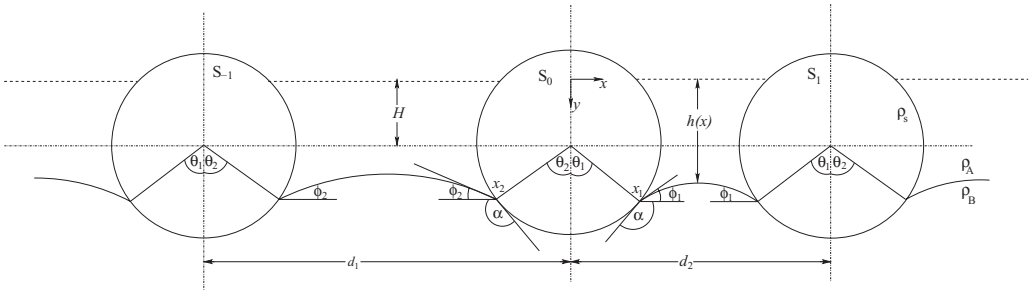

FIG. 3. Parallel cylinders of equal radius R separated by center-to-center distances d_1 and d_2 floating at an interface separating fluids A and B.

of Eqs. (7) and (18)–(20) and the Nicolson approximation. The Bond number, B is set at 0.001 and the contact angle is varied from 45° to 135°. At small distances, the agreement between the asymptotic result (29), the Nicolson approximation, and the numerical solution is excellent. But at larger separation distances, deviations can be noticed between the present result and the numerical solution. It is interesting to note that the Nicolson approximation agrees well with the numerical solution even for these separation distances. Clearly, the $\mathcal{O}(B^3)$ difference between Eqs. (29) and (32) is responsible for this discrepancy. This suggests that the recovery of the Nicolson approximation can be obtained by carrying out a double expansion in $B^{1/2}$ and d/l_c (or equivalently $B^{1/2}$ and d/R), which is beyond the scope of this paper. Nevertheless, the present asymptotic approach highlights the essential physics of capillary attraction by carefully examining various contributions to the horizontal force.

IV. CAPILLARY ATTRACTION WITH AN ARRAY OF CYLINDERS

As mentioned in the Introduction, in most applications two particles are seldom found in isolation: rather islands of close packed particles are commonly encountered. In this section, we calculate the force of attraction for an infinite array of identical cylinders. To the best of our knowledge, all previous studies involving many particles use a vector superposition of forces by considering two particles at a time[8–10,55] and the present geometry has not been studied before. The starting point of our analysis is a configuration of an infinite array of equally spaced cylinders on an interface, with spacing d_0 between the cylinders. For identical cylinders, the vertical and horizontal force balance equations (7) and (8) show that each cylinder is influenced by the interface shape in its immediate neighborhood. In this configuration of a uniform lattice, the meniscus shapes on either side of each cylinder are identical and hence each cylinder experiences an equal and opposite lateral force from its two neighbors. But this configuration is an unstable equilibrium and any perturbation from this state will result in a force imbalance and generate non-zero net lateral forces, leading to aggregation. Let us consider a specific disturbance where one of the cylinders, say S_0, is slightly disturbed from this equilibrium as shown in Figure 3 such that average distance $d_0 = (d_1 + d_2)/2$. Without loss of generality, let us assume that $d_1 > d_2$. This will generate a net attractive force between S_0 and S_1. Similarly, S_{-1} will experience a net attractive force toward S_{-2}. The present configuration is equivalent to a periodically extended perturbed lattice, and hence cylinders S_n and $S_{n\pm2}$ are identical. It is worth emphasizing that the present geometry is not the same as considering three cylinders in isolation, i.e., the interface shape does not become flat on either side of cylinders $S_{\pm1}$.

It is sufficient to calculate the net force experienced by any one cylinder in the array. Owing to periodicity of the lattice, the same magnitude of force acts on all the cylinders. Even though capillary forces are non-local in nature, it is sufficient to consider only three cylinders as shown in Figure 3. Without loss of generality, we can choose the origin to lie at S_0. All other variables have the same meaning as before. As discussed before, when the cylinders form a perfect lattice, i.e., $d_1 = d_2$, the net force of attraction vanishes. Hence, the force of attraction will depend on the parameter

$\delta = (d_1 - d_2)/2$. Introducing the non-dimensional variables $d_i^* = d_i/R$, $(i = 0, 1, 2)$, $\delta^* = \delta/R$ and solving for the interface shape (Eq. (11)) with boundary conditions at the contact lines, we get four equations

$$x_1^* = \sin(\theta_1), \qquad x_2^* = \sin(\theta_2), \tag{33}$$

$$B^{1/2}[H^* + \cos(\theta_2)] \sinh\left((d_1^* - 2x_2^*)B^{1/2}\right) = \tan(\phi_2)\left[1 + \cosh\left((d_1^* - 2x_2^*)B^{1/2}\right)\right], \tag{34}$$

$$B^{1/2}[H^* + \cos(\theta_1)] \sinh\left((d_2^* - 2x_1^*)B^{1/2}\right) = \tan(\phi_1)\left[1 + \cosh\left((d_2^* - 2x_1^*)B^{1/2}\right)\right]. \tag{35}$$

The expansions (21)–(25) are substituted into Eqs. (7) and (33)–(35) and the resulting equations are satisfied at every order. After some algebra, the final expression for the force of attraction between cylinders per unit length is found to be

$$F^* = \frac{B^2\chi^2}{2}\left(\frac{\delta^*}{d_0^*}\right)\left[1 - \frac{B}{6}\left\{d_0^{*2} - \delta^{*2} + 6\sin^2\alpha - \frac{1}{d_0^*}\left(6\chi\cos\alpha + 20\sin^3\alpha\right)\right\}\right] + \mathcal{O}(B^{7/2}). \tag{36}$$

As discussed earlier in this section, the force of attraction clearly depends on the average particle distance d_0^* and the variation of separation distance, δ^*. If $\delta^* = 0$, the particles are arranged in a perfect "lattice" and the net horizontal force vanishes. But for a disturbed lattice, $\delta^* \neq 0$, and the expression for force does not lend itself to a simple interpretation. Since $B \ll 1$ and $d_0^* > 0$, the sign of F is determined by δ^*. Hence, when $\delta^* > 0$ $(\delta^* < 0)$, $F > 0$ $(F < 0)$ which makes cylinder S_0 move toward S_1 (S_{-1}). The effect of a non-zero force would be to make each cylinder move toward its left or right neighbor depending on whether $\delta^* > 0$ or $\delta^* < 0$, respectively. This "binary" attraction then reduces the number of "effective" particles by a factor of 2. This process would presumably continue until all the particles clump together into a sheet of closely spaced cylinders.

A. Elasticity of an interface with particles

We can compare the results obtained in this section to the two cylinder case considered in Sec. III. We do this by comparing the effective Gibbs elasticity or dilational modulus for a fixed surface coverage. In both the cases, the surface coverage, ϕ, analogous to the volume frame in a bulk suspension depends solely on the separation distance, d for the two cylinder case, and d_0 for the array case. But in the latter case, the degree of clustering can change with δ. For $\delta = 0$, the particles are uniformly spaced resulting in no net force of attraction. And when $\delta = 2R$, we have binary clusters, i.e., the array comprises of pairs of cylinders in contact, each pair separated from its neighbor with an average distance d_0.

The Gibbs elasticity or dilational modulus is defined as[56]

$$\varepsilon = \frac{\partial\sigma_{app}}{\partial(lnA)}, \tag{37}$$

where σ_{app} is the apparent surface tension, and A is the surface area of the interface. As discussed by Lucassen,[56] this reduces to the following expression:

$$\varepsilon = \left|\frac{\partial F}{\partial d}\right|. \tag{38}$$

For the two cylinder case, the Gibbs elasticity is obtained by Eqs. (29) and (38)

$$\varepsilon_{\text{pair}} = \frac{\sigma B^{5/2}\chi^2}{2R}\left[1 - B^{1/2}d^*\right] + \mathcal{O}(B^{7/2}). \tag{39}$$

Similarly, for the case of an array of cylinders, the Gibbs elasticity is obtained by differentiating F^* in Eq. (36) with d_0^*. By choosing $d^* = d_0^*$, the ratio, $\varepsilon_{\text{arr}}/\varepsilon_{\text{pair}}$ compares the elasticity of an interface covered with particles interacting with each other simultaneously given by Eq. (36), to that

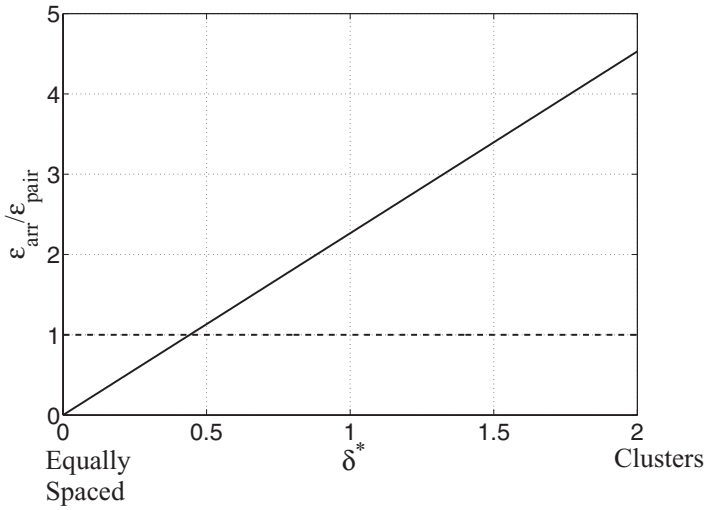

FIG. 4. Comparison of Gibbs elasticity between the two cylinder case and for an array of cylinders for a fixed surface coverage. The average separation distance in both the cases is $d_0^* = 4$, and $B = 0.001$, $D = 2$ and $\alpha = 135^\circ$.

obtained by using pair-wise interactions between pairs of cylinders. For a fixed separation distance of $d^* = d_0^* = 4$, Figure 4 shows the variation of Gibbs elasticity of an interface with an array of cylinders as a function of the parameter δ. As the clustering of particles increases, the effective Gibbs elasticity increases.

The above results again shows that there are important differences between two isolated cylinders and an array of cylinders. Dense interfacial suspensions are closer to the array model considered in this section. Therefore, this can have important implications in modeling rheology of dense interfacial suspensions of particles.

V. CYLINDER ON A CURVED INTERFACE

We now consider the case of particles on a curved interface, first by calculating the force on a single particle and then calculating the capillary attraction force between two particles on a curved interface. A floating cylinder on a flat interface experiences no lateral force because of symmetric deformation of the interface on either side of the particle. But recent experiments have shown that particles on curved interfaces experience a lateral force. Hu and Bush[49] have shown that tiny beetle larvae use curvature gradients to propel themselves on a fluid meniscus. Cavallaro *et al.*[50] use curvature gradients to migrate rod-like particles with the aim of creating complex particle rafts. The contact angle in their experiments was 120° and the particles aligned perpendicular to the direction of motion. In this section, we develop an asymptotic theory valid for small particles floating on arbitrary curved interface and our results have direct relevance to the experiments discussed above.

Consider a curved interface as shown in Figure 5(a), where $\eta(\xi)$ is the height of the interface from a known reference. The background curvature provides a capillary pressure contribution to the pressure balance on the interface. The presence of particles distorts the background interface modifying the local curvature around the particles. The gravitational force can be resolved along and perpendicular to the background interface as shown in Figure 5(b), where γ is the angle made by the normal to the undisturbed interface with the vertical. We assume that the radius of the cylinders is small compared to the characteristic length scale of the background, the latter being typically $\mathcal{O}(l_c)$. This is equivalent to the Bond number being small, and hence the interface distortion due to the particle will be small compared to capillary length. In this limit, we can linearize the interface deformation about the undistorted curved interface and derive a simple expression for the perturbed curvature of the interface as shown in the Appendix. The perturbed curvature is in turn used to derive

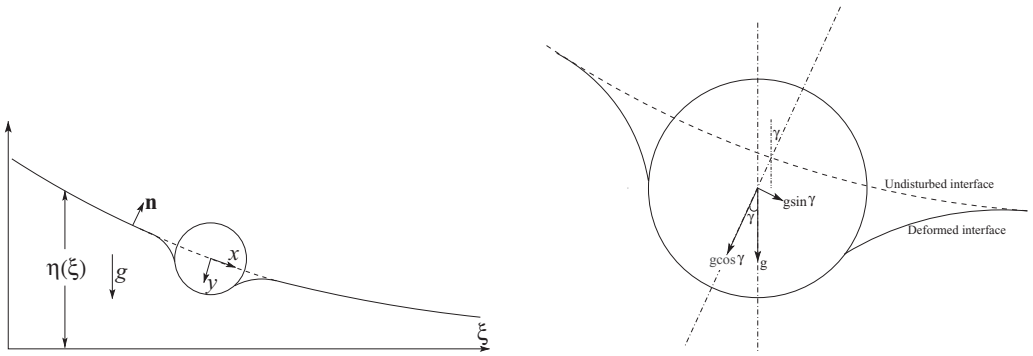

(a) (b)

FIG. 5. (a) Cylinder floating on a curved interface in the presence of gravity. (b) Gravity resolved into normal and tangential components for a each cylinder.

a perturbed Young-Laplace equation which can be written in dimensional form as

$$h_{xx} + a(\xi)h_x + b(\xi)h = 0, \tag{40}$$

where (x, y) is the local coordinate system defined along and perpendicular to the interface lying along the undisturbed interface as shown in Figure 5(a), a and b are parameters characterizing the background interface. Due to the small size of the particles, we calculate $a(\xi)$ and $b(\xi)$ at the origin of the local coordinate system, $x = 0$. This allows us to obtain a simple solution to the above equation instead of a power series solution. The general solution takes the simple form

$$h(x) = c_1 e^{\lambda_- x} + c_2 e^{\lambda_+ x}, \tag{41}$$

where the relation between the eigenvalues, $\lambda_\pm$, and interface shape parameters like curvature and slope are given in the Appendix. Due to the curvature of the background interface, the interface distortion is not symmetric on either side of the particle, leading to a lateral force. We non-dimensionalize the eigenvalues $\lambda_\pm$ with the capillary length, and (x, y) with the radius of the particle. The interface shape on either side of the cylinder is given by the solution of Eq. (A8) with contact angle boundary conditions on the surface of the cylinder

$$h^*(x^*) = \begin{cases} -B^{-1/2}\dfrac{\tan\phi_1}{\lambda_-^*} e^{B^{1/2}\lambda_-^*(x^* - x_1^*)} & (x^* \geq x_1^*), \\ B^{-1/2}\dfrac{\tan\phi_2}{\lambda_+^*} e^{B^{1/2}\lambda_+^*(x^* + x_2^*)} & (x^* \leq -x_2^*), \end{cases} \tag{42}$$

where $\lambda_\pm^* = l_c\lambda_\pm$. The horizontal and vertical positions of the contact lines are geometrically related to the wetting angles, which yields the following relations:

$$x_1^* = \sin(\theta_1), \tag{43}$$

$$x_2^* = \sin(\theta_2), \tag{44}$$

$$B^{1/2}(H^* + \cos(\theta_1)) = -\frac{\tan\phi_1}{\lambda_-^*}, \tag{45}$$

$$B^{1/2}(H^* + \cos(\theta_2)) = \frac{\tan\phi_2}{\lambda_+^*}. \tag{46}$$

The resultant normal force balance is given by

$$B\omega^2 \left\{\theta_1 + \theta_2 + \frac{1}{2}\left[\sin(2\theta_1) + \sin(2\theta_2)\right] + 2H^*\left[\sin(\theta_1) + \sin(\theta_2)\right]\right\}$$
$$= 2\left[\sin(\alpha + \theta_1) + \sin(\alpha + \theta_2)\right] + 2\pi B\omega^2 D, \tag{47}$$

and the tangential force balance is given by

$$F^* = \frac{F}{\sigma} = F_c^* + F_w^*, \tag{48}$$

where $\omega^2 = \cos\gamma$

$$F_c^* = \cos(\alpha+\theta_2) - \cos(\alpha+\theta_1) + B\omega^2 \left\{ H^*(\cos\theta_1 - \cos\theta_2) + \frac{\left(\sin^2\theta_2 - \sin^2\theta_1\right)}{2} \right\}, \tag{49}$$

$$F_w^* = \pi B_s (1-\omega^4)^{1/2}. \tag{50}$$

Note that the effective gravity normal to a curved interface is $g' = g\cos\gamma$ which reduces the net buoyancy force. The effective Bond number is now $B\omega^2$. In the above equations, F_c^* is the curvature contribution, F_w^* is the component of weight of the particle tangential to the interface, and $B_s = g\rho_s R^2/\sigma$ is the Bond number based on the density of the solid particle. The above Eqs. (47) and (48) are identical to the vertical and horizontal force balance equations (7) and (8), respectively, except for the modification of the Bond number. Expanding the above equations in powers of $B^{1/2}$ and following the procedure outlined in Sec. III, the lateral curvature force due to gravity is given by

$$F_c^* = \frac{B^2\omega^4\chi^2(\lambda_+^* + \lambda_-^*)}{2(\lambda_+^* - \lambda_-^*)} \left[1 + 2B^{1/2}\sin\alpha \left(\frac{\lambda_+^*\lambda_-^* - \omega^2}{\lambda_+^* - \lambda_-^*} \right) \right] + \mathcal{O}(B^3). \tag{51}$$

In terms of the interface shape, the contribution from the weight for the particle can be written as

$$F_w^* = -\pi B_s \sin\gamma, \tag{52}$$

and the lateral curvature force simplifies to the form

$$F_c^* = \frac{B^2\chi^2\cos^2\gamma\kappa^*\tan\gamma}{2(4\kappa^{*2} + 5\kappa^{*2}\tan^2\gamma + 4\kappa_{\xi^*}^*\sin\gamma + 4\cos\gamma)^{1/2}} \left\{ 1 - B^{1/2} \frac{2\sin\alpha\left[\kappa^{*2}\sec^2\gamma + \kappa_{\xi^*}^*\sin\gamma + 2\cos\gamma\right]}{(4\kappa^{*2} + 5\kappa^{*2}\tan^2\gamma + 4\kappa_{\xi^*}^*\sin\gamma + 4\cos\gamma)^{1/2}} \right\} + \mathcal{O}(B^3), \tag{53}$$

where $\kappa^* = \kappa l_c$. The dominant contribution to the total lateral force comes from the weight of the particle. Since the denominator in Eq. (53) is positive and $B^{1/2}$ is small, it is also clear that the sign of the curvature contribution to the force, F_c^*, depends on the product of the curvature and the slope of the interface.

To quantify the above result, we consider a simple example. Consider a cylinder floating on a catenoid given by the formula

$$\eta^* = \cosh(\xi^*), \tag{54}$$

where $(\xi^*, \eta^*) = (\xi/l_c, \eta/l_c)$. The curvature is given by $\kappa^* = \mathrm{sech}^2(\xi^*)$. Figure 6 shows the lateral force experienced by a floating cylinder. The gravitational curvature contribution, F_c^* is clearly small compared to the weight of the particle, F_w^*. It is also interesting to note that the shape of the curvature contribution, F_c^* obtained here has a striking similarity with the variation of gradient of curvature for this interface.

VI. CAPILLARY ATTRACTION ON A CURVED INTERFACE

We now treat the case of attraction between horizontal cylinders floating on an interface with a finite background curvature, the motivation for which was given in the Introduction. Consider two cylinders on an interface with a known background curvature as shown schematically in Figure 7, where the dashed curve represents the undisturbed interface in the absence of particles. We use the same perturbed Young-Laplace equation, (40), as used in Sec. V but with the origin of the local coordinate system (x, y) now lying on the undisturbed interface midway between the two particles. The coefficients $a(\xi)$ and $b(\xi)$ in Eq. (40) are evaluated at the origin of the local coordinate system,

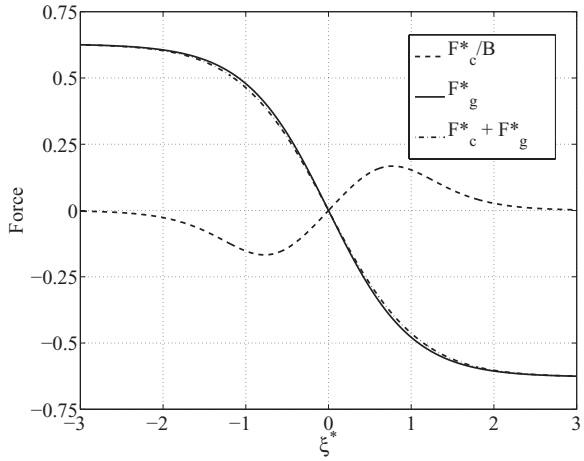

FIG. 6. Lateral force on a cylinder floating on a catenoid, with $\alpha = 135^\circ$, $B = 0.1$, $D = 2$ and $B_s = 0.2$. The three curves represent curvature contribution (dotted line), gravitational contribution (solid line), and the total force (dashed-dotted line).

$x = 0$. We assume that the separation distance, d, between the particles is much smaller than the capillary length, i.e., $d \sim \mathcal{R} \ll l_c$. In this limit, both the particles experience approximately the same lateral force due to gravitational and curvature effects, and hence do not contribute toward capillary attraction between the particles. But since the particles are located at distances $\pm d/2$, there are key differences between the curved interface case and a flat interface. This will be discussed later in the section.

We now solve for interface distortion from the undisturbed interface by again invoking symmetry conditions midway between the cylinder. For a curved background interface, this will not be strictly true, but since the separation distance between particles is small, i.e., $d \ll l_c$, any asymmetry due to curvature of the background interface should be a higher order effect. We again non-dimensionalize the eigenvalues $\lambda_\pm$ with the capillary length, and (x, y) with the radius of the particle. Hence, the interface shape on either side of cylinder S_1 in non-dimensional form can be written as

$$h^*(x^*) = \begin{cases} B^{-1/2}\dfrac{\tan\phi_1 e^{B^{1/2}\lambda_0^*(x^*+x_1^*)}}{\lambda_0^{*2}-\epsilon^{*2}}\left[\lambda_0\dfrac{\sinh(B^{1/2}\epsilon^* x^*)}{\sinh(B^{1/2}\epsilon^* x_1^*)} - \epsilon\dfrac{\cosh(B^{1/2}\epsilon^* x^*)}{\sinh(B^{1/2}\epsilon^* x_1^*)}\right] & (-x_1^* \le x^* \le x_1^*), \\ B^{-1/2}\dfrac{\tan\phi_2}{\lambda_+^*} e^{B^{1/2}\lambda_+^*(x^*+x_2^*)} & (x^* \le -x_2^*), \end{cases} \tag{55}$$

where $\lambda_0^* = (\lambda_+^* + \lambda_-^*)/2$ and $\epsilon^* = (\lambda_+^* - \lambda_-^*)/2$. The x- and y- locations of the contact lines give us four additional relations

$$x_1^* = \frac{d^*}{2} - \sin\theta_1, \tag{56}$$

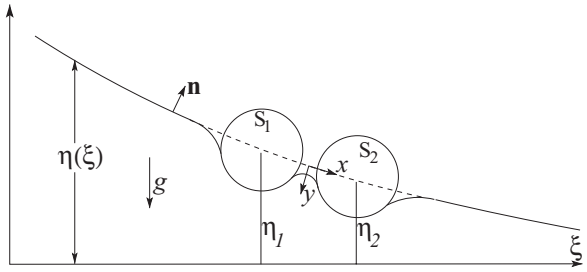

FIG. 7. Capillary attraction on an arbitrary curved interface. (ξ, η) are the coordinates used to describe the background curved interface, and (x, y) are the local coordinates at the location of the particles.

$$x_2^* = \frac{d^*}{2} + \sin\theta_2, \tag{57}$$

$$B^{1/2}(H^* + \cos\theta_1)\tanh(B^{1/2}\epsilon^* x_1^*) = \frac{-\tan\phi_1}{\lambda_0^{*2} - \epsilon^{*2}}\left[\epsilon^* + \lambda_0^* \tanh(B^{1/2}\epsilon^* x_1^*)\right], \tag{58}$$

$$B^{1/2}(H^* + \cos\theta_1) = \frac{\tan\phi_2}{\lambda_0^* + \epsilon^*}. \tag{59}$$

In deriving the above equations, the background interface parameters, λ_0^* and ϵ^*, are evaluated midway between the particles, $x = 0$, and not at the location of the contact lines x_1^* and x_2^*. As a result an asymmetric term, $(\lambda_0^* + \epsilon^*)$, enters the analysis. The normal and tangential force balance equations for each cylinder are the same as used in Sec. V, and hence we do not repeat them here. Expanding Eqs. (47), (48), and (56)–(59) simultaneously in powers of $B^{1/2}$ and following the solution procedure outlined in Sec. III, the resultant expression for force of attraction can be written as

$$F_l^* = \frac{B^2\omega^4\chi^2}{2}\left\{1 + \frac{2B^{1/2}}{\lambda_0^* + \epsilon^*}\left[\left(\frac{d^*}{2} - \sin\alpha\right)\left(\lambda_0^{*2} - \epsilon^{*2}\right) - \omega^2\sin\alpha\right]\right\} + \mathcal{O}(B^3), \tag{60}$$

where the subscript l denotes that this expression is valid for the left cylinder, S_1. In terms of curvature and slope of the background interface, the force of attraction can be simplified to the form

$$F_l^* = \frac{B^2\chi^2\cos^2\gamma}{2}\left\{1 - 2B^{1/2}\frac{\left\{(d^* - 2\sin\alpha)\left(\kappa^{*2}\sec^2\gamma + \kappa_{\xi^*}^*\sin\gamma\right) + d^*\cos\gamma\right\}}{\left[\kappa^*\tan\gamma + \sqrt{4\kappa^{*2} + 5\kappa^{*2}\tan^2\gamma + 4\kappa_{\xi^*}^*\sin\gamma + 4\cos\gamma}\right]}\right\} + \mathcal{O}(B^3). \tag{61}$$

A similar analysis can be carried out to evaluate the force of attraction on the right cylinder, S_2. For brevity, we only state the final result

$$F_r^* = -\frac{B^2\chi^2\cos^2\gamma}{2}\left\{1 + 2B^{1/2}\frac{\left\{(d^* - 2\sin\alpha)\left(\kappa^{*2}\sec^2\gamma + \kappa_{\xi^*}^*\sin\gamma\right) + d^*\cos\gamma\right\}}{\left[\kappa^*\tan\gamma - \sqrt{4\kappa^{*2} + 5\kappa^{*2}\tan^2\gamma + 4\kappa_{\xi^*}^*\sin\gamma + 4\cos\gamma}\right]}\right\} + \mathcal{O}(B^3). \tag{62}$$

The two forces, F_l^* and F_r^*, give the unbalanced forces on the left and right cylinders, respectively. The net force of attraction between the cylinders is given by

$$F_c^* = \frac{F_l^* - F_r^*}{2}. \tag{63}$$

The above expressions, (61)–(63), reduce to that obtained for a flat interface in the limit $\kappa \to 0$, $\eta_\xi \to 0$, and $\gamma \to 0$. The leading term in the expression for forces involves the angle γ, and not the curvature. This suggests that the dominant role of a curved interface is from the variation of the slope of the interface rather than a direct influence of curvature. The slope of the interface modifies the effective gravity reducing the potential for capillary attraction.

As an application of these results, consider a simple case of two cylinders floating on a catenoid given by the formula

$$\eta^* = \cosh(\xi^*), \tag{64}$$

where $(\eta^*, \xi^*) = (\eta/l_c, \xi/l_c)$ and $\kappa^* = \kappa l_c$. The effects of curvature of the background interface on the force of attraction can be estimated by normalizing the force of attraction with the force obtained by using the Nicolson approximation, Eq. (32), for cylinders on a flat interface. For a catenoid interface, this ratio is evaluated for three different separation distances as shown in Figure 8. Clearly,

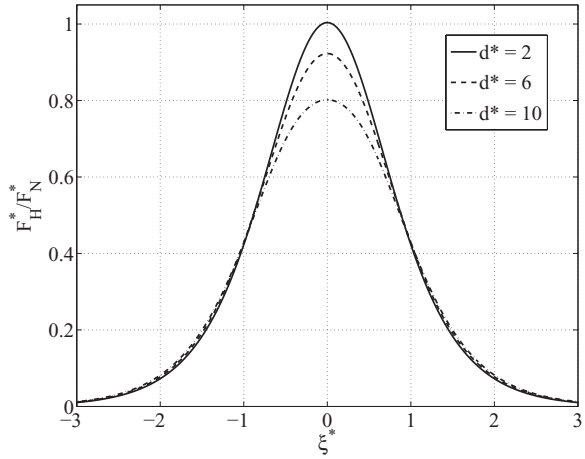

FIG. 8. The net force of attraction, F^*_H, between the two cylinders floating on a catenoid interface with $B = 0.001$, $D = 2$, $\alpha = 135^\circ$ normalized by the force obtained by Nicolson approximation for a flat interface, and for three different separation distances.

an increase in separation distance reduces the force of attraction for a curved interface relative to that for a flat interface, as is evident from Eqs. (61)–(63).

VII. SUMMARY AND CONCLUSION

In this study, we have obtained asymptotic solutions for the capillary attraction force between parallel cylinders for three configurations, (i) attraction between two cylinders on a flat interface, (ii) attraction between two cylinders on a curved interface, and (iii) attraction forces in an array of cylinders. Using a systematic perturbation expansion at small Bond number, the present study places the established Nicolson approximation on a firm footing, thus lending confidence to the use of the Nicolson approximation for other particle shapes. Moreover, no constraints were imposed on the vertical position or angular orientations of the particles. Particles on a curved interface distort the interface modifying the surface pressure balance. A perturbed Young-Laplace equation was obtained governing the perturbations to the interface. Unlike the case of a flat interface, even a single particle experiences a lateral force, due to both gravity along the interface and to the effects of background curvature. The effect of gravity is straightforward and causes the particles to slide toward regions of lower elevation. But the effect of curvature does not lend itself to a simple interpretation.

Since the present analysis is for a static case, we expect that in a quasi-static scenario, the vertical and angular orientations of the cylinders will change as the particles approach each other. The analysis reveals that for small Bond numbers, the magnitude of vertical and angular shift is small, and may not be too relevant for the dynamics of freely floating particles.

The above analysis has been carried out for horizontal parallel cylinders. In reality, such configurations are rarely encountered as cylinders seldom remain parallel to each other. Nonetheless, the present analysis highlights the essential physics involved in the capillary attraction process. The infinite cylinder problem showed the essential mechanism behind formation of particle clusters at a fluid interface. When the particle concentration is large, these clusters can completely cover the interface, thus modifying the boundary conditions for the bulk flow.

We conclude this paper by briefly discussing experiments on related geometries. There are only a few experimental results where attempts have been made to verify Nicolson's approximation. Velev *et al.*[6] verified Nicolson's approximation by measuring the force of attraction between two vertical cylinders whereas Dushkin *et al.*[7] measured force of attraction between vertical rods and spheres. In the latter experiments, it is not clear if the spheres are allowed a vertical degree of freedom. And more importantly, as the particles move, they experience a viscous drag. Some preliminary

experiments with glass spheres show that viscous drag force is comparable to capillary attraction force[57] and has a non-trivial dependence on the viscosity of the fluid.[58]

ACKNOWLEDGMENTS

We gratefully acknowledge funding from the Natural Science and Engineering Research Council (NSERC) of Canada.

APPENDIX: DERIVATION OF A PERTURBED YOUNG-LAPLACE EQUATION

In this appendix, we derive an equation governing perturbations on a known background interface caused by the presence of particles. We call the resulting equation as the perturbed Young-Laplace equation. In the absence of particles, the dimensional Young-Laplace equation for the background interface can be written as

$$(\rho_B - \rho_A) g \eta(\xi) = \sigma \kappa(\xi), \tag{A1}$$

where η is the height of the interface measure from a known reference where the interface is flat, $\kappa(\xi) = (\nabla \cdot \mathbf{n})$ is the curvature of the background interface, ξ is the horizontal coordinate. For a planar interface, κ takes the form

$$\kappa = \frac{\eta_{\xi\xi}}{(1+\eta_\xi^2)^{3/2}}. \tag{A2}$$

The shape of the background interface, $\eta(\xi)$ can be determined from the solution of equation (A1) with suitable boundary conditions. To account for perturbations to the background interface caused by the presence of particles, we define a local coordinate axis (x, y), tangential and normal to the interface with the origin in the vicinity of the particles, and lying on the undisturbed interface. The perturbation to the background interface in the normal direction, y scales with the radius of the particle, whereas the interface elevation, η, scales with the capillary length. In the limit $B \ll 1$, we therefore have $h \ll \eta$. Defining γ as the angle made by the normal to the background interface with the vertical, defined in an anti-clockwise sense, we have

$$\eta' = \eta + y \cos\gamma. \tag{A3}$$

It can be easily shown that $d\gamma/dx = \kappa$. It is useful to express the background curvature in terms of the arc-length coordinate, x,

$$\kappa = \frac{\eta_{xx}}{\left(1-\eta_x^2\right)^{1/2}}. \tag{A4}$$

Substituting η' into Eq. (A4) and considering only terms linear in h, the perturbed curvature reduces to

$$\kappa' = \kappa + \frac{\cos\gamma}{(1-\eta_x^2)^{1/2}} h_{xx} + \left[\frac{\kappa\eta_x\cos\gamma}{(1-\eta_x^2)} - \frac{2\kappa\sin\gamma}{(1-\eta_x^2)^{1/2}}\right] h_x - \left[\frac{\kappa^2\sin\gamma\eta_x}{(1-\eta_x^2)} + \frac{\kappa^2\cos\gamma + \kappa_x\sin\gamma}{(1-\eta_x^2)^{1/2}}\right] h + \mathcal{O}(h^2). \tag{A5}$$

From the Young-Laplace equation at the perturbed interface, we have $(\rho_B - \rho_A) g \eta' = \sigma\kappa'$. On simplifying and eliminating the contribution from the background interface, the perturbed Young-Laplace equation for the perturbation becomes

$$h_{xx} + a h_x + b h = 0, \tag{A6}$$

$$a = -\kappa \tan\gamma, \tag{A7}$$

$$b = -\left[\kappa^2 \sec^2\gamma + \kappa_\xi \sin\gamma + \frac{\cos\gamma}{l_c^2}\right]. \tag{A8}$$

In the above equation, the second term represents the effect of background curvature whereas the last term represents the gravitational contribution normal to the interface. Since the above equation involves coefficients which depend on the independent variable, a general solution should be obtained by a power-series method if the background interface is known *a priori*. When the extent of perturbation caused by particles is small compared to the characteristic length scale of the background interface, we can assume that the particles locally do not sense the variation of curvature of the background interface. This is similar in spirit to the β-plane approximation commonly used on geophysical flows where the Coriolis frequency is assumed to vary linearly from a specified value at a given latitude. We, therefore, assume that coefficients a and b assume a constant value at the scale of separation of two particles. Since $d \ll l_c$, this is a reasonable assumption. In this case, the general solution of Eq. (A8) is

$$h(x) = c_1 \exp(\lambda_- x) + c_2 \exp(\lambda_+ x), \tag{A9}$$

where $\lambda_\pm = -\frac{1}{2}\left(a \mp \sqrt{a^2 - 4b}\right)$.

[1] G. M. Whitesides and B. Grzybowski, "Self-assembly at all scales," Science **295**, 2418–2421 (2002).
[2] D. Vella and L. Mahadevan, "The Cheerios effect," Am. J. Phys. **73**, 819–825 (2005).
[3] P. Pieranski, "Two-dimensional interfacial colloidal crystals," Phys. Rev. Lett. **45**, 569–572 (1980).
[4] L. Bragg and J. F. Nye, "A dynamical model of a crystal structure," Proc. R. Soc. London, Ser. A **190**, 474–481 (1947); L. Bragg and W. M. Lomer, "A dynamical model of a crystal structure. II," *ibid.* **196**, 171–181 (1949).
[5] J. T. Petkov, N. D. Denkov, K. D. Danov, O. D. Velev, R. Aust, and F. Durst, J. Colloid Interface Sci. **172**, 147–154 (1995).
[6] O. D. Velev, N. D. Denkov, V. N. Paunov, P. A. Kralchevsky, and K. Nagayama, "Direct measurement of lateral capillary forces," Langmuir **9**, 3702–3709 (1993).
[7] C. D. Dushkin, P. A. Kralchevsky, H. Yoshimura, and K. Nagayama, "Lateral capillary forces measured by torsion microbalance," Phys. Rev. Lett. **75**, 3454–3457 (1995).
[8] N. D. Vassileva, D. Ende, F. Mugele, and J. Mellema, "Capillary forces between spherical particle," Langmuir **21**, 11190–11200 (2005).
[9] M. Dalbe, D. Cosic, M. Berhanu, and A. Kudrolli, "Aggregation of frictional particles due to capillary attraction," Phys. Rev. E **83**, 051403 (2011).
[10] P. A. Kralchevsky and K. Nagayama, *Particles at Fluids Interfaces and Membranes* (Elsevier, Amsterdam, 2001).
[11] H. M. Princen, "The equilibrium shape of interfaces, drops, and bubbles. Rigid and deformable particles at interfaces," in *Surface and Colloid Science*, edited by E. Matijevic (Interscience, New York, 1969), Vol. 2, pp. 1–84.
[12] G. Y. Onoda, "Direct observation of two-dimensional, dynamical clustering and ordering with colloids," Phys. Rev. Lett. **55**, 226–229 (1980).
[13] W. Ramsden, "Separation of solids in the surface-layers of solutions and 'suspensions' (observations on surface-membranes, bubbles, emulsions and mechanical coagulation)–Preliminary account," Proc. R. Soc. London **72**, 156–164 (1903).
[14] S. U. Pickering, "Emulsions," J. Chem. Soc. Trans. **91**, 2001–2021 (1907).
[15] J. A. Kitchener and P. R. Mussellwhite, "The theory of stability of emulsions," in *Emulsion Science*, edited by P. Sherman (Academic, New York, 1968), pp. 77–130.
[16] P. Kruglyakov and A. Nushtayeva, "Emulsions stabilized by solid particles: The role of capillary pressure in the emulsion films," in *Emulsions: Structure, Stability and Interactions*, Interface Science and Technology Vol. 4, edited by D. N. Petsev (Elsevier Science, Amsterdam, 2004), pp. 641–676.
[17] B. P. Binks, "Particles as surfactants–similarities and differences," Curr. Top. Colloid Interface Sci. **7**, 21–41 (2002).
[18] A. D. Dinsmore, M. F. Hsu, M. G. Nikolaides, M. Marquez, A. R. Bausch, and D. A. Weitz, "Colloidosomes: Selectively permeable capsules composed of colloidal particles," Science **298**, 1006–1009 (2002).
[19] A. B. Subramaniam, M. Abkarian, and H. A. Stone, "Controlled assembly of jammed colloidal shells on fluid droplets," Nature Mater. **4**, 553–556 (2005).
[20] N. D. Denkov, O. D. Velev, P. A. Kralchevsky, I. B. Ivanov, H. Yoshimura, and K. Nagayama, "Two-dimensional crystallization," Nature (London) **361**, 26 (1993).
[21] A. B. Subramaniam, M. Abkarian, L. Mahadevan, and H. A. Stone, "Non-spherical bubbles," Nature (London) **438**, 930 (2005).
[22] R. Miller, V. B. Fainerman, V. I. Kovalchuk, D. O. Grigoriev, M. E. Leser, and M. Michel, "Composite interfacial layers containing micro-size and nano-size particles," Adv. Colloid Interface Sci. **128–130**, 17–26 (2006).
[23] D. Vella, P. Aussillous, and L. Mahadevan, "Elasticity of an interfacial particle raft," Europhys. Lett. **68**, 212–218 (2004).
[24] T. Okubo, "Surface tension of structured colloidal suspensions of polystyrene and silica spheres at air-water interface," J. Colloid Interface Sci. **171**, 55–62 (1995).
[25] L. Dong and D. Johnson, "Interfacial tension measurements of colloidal suspensions: An explanation of colloidal particle-driven interfacial flows," Adv. Space Res. **32**, 149–153 (2003).
[26] P. Cicuta, E. J. Stancik, and G. G. Fuller, "Shearing or compressing a soft glass in 2D: Time-concentration superposition," Phys. Rev. Lett. **90**, 236101 (2003).

[27] V. B. Fainerman, V. I. Kovalchuk, E. H. Lucassen-Reynders, D. O. Grigoriev, J. K. Ferri, M. E. Leser, M. Michel, R. Miller, and H. Möhwald, "Surface-pressure isotherms of monolayers formed by microsize and nanosize particles," Langmuir **22**, 1701–1705 (2006).
[28] J. T. Davies and E. K. Rideal, *Interfacial Phenomena* (Academic, New York, 1961).
[29] M. M. Nicolson, "The interaction between floating particles, "Proc. Cambridge Philos. Soc. **45**, 288–295 (1949).
[30] W. A. Gifford and L. E. Scriven, "On the attraction of floating particles," Chem. Eng. Sci. **26**, 287–297 (1971).
[31] D. Y. C. Chan, J. D. Henry, Jr., and L. R. White, "The interaction of colloidal particles collected at a fluid interface," J. Colloid Interface Sci. **79**, 410–418 (1981).
[32] C. Allain and M. Cloitre, "Interaction between particles trapped at fluid interfaces. II. Free-energy analysis of the interaction between two horizontal cylinders," J. Colloid Interface Sci. **157**, 269–277 (1993).
[33] P. A. Kralchevsky, V. N. Paunov, I. B. Ivanov, and K. Nagayama, "Capillary meniscus interaction between colloidal particles attached to a liquid-fluid interface," J. Colloid Interface Sci. **151**, 79–94 (1992).
[34] V. N. Paunov, P. A. Kralchevsky, N. D. Denkov, and K. Nagayama, "Lateral capillary forces between floating submillimeter particles," J. Colloid Interface Sci. **157**, 100–112 (1993).
[35] C. Allain and M. Cloitre, "Interaction between particles trapped at fluid interfaces. I. Exact and asymptotic solutions for the force between horizontal cylinders," J. Colloid Interface Sci. **157**, 261–268 (1993).
[36] See supplementary material at http://dx.doi.org/10.1063/1.4769758 for experimental study of the effect of surface-adsorbed hydrophobic particles on the Landau-Levich law.
[37] L. Landau and B. Levich, "Dragging of a liquid by a moving plate," Acta Physicochim. USSR **17**, 42–54 (1942).
[38] C.-W. Park and G. M. Homsy, "Two-phase displacement in Hele Shaw cells: Theory," J. Fluid Mech. **139**, 291–308 (1984).
[39] J. Ratulowski and H. C. Chang, "Maragoni effects of trace impurities on the motion of long gas bubbles in capillaries," J. Fluid Mech. **210**, 303–328 (1990).
[40] C.-W. Park, "Effects of insoluble surfactants on dip coating," J. Colloid Interface Sci. **146**, 382–394 (1991).
[41] K. J. Stebe and D. Barthès-Biesel, "Marangoni effects of adsorption-desorption controlled surfactants on the leading end of an infinitely long bubble in a capillary," J. Fluid Mech. **286**, 25–48 (1995).
[42] R. Krechetnikov and G. M. Homsy, "Experimental study of substrate roughness and surfactant effects on the Landau-Levich law," Phys. Fluids **17**, 102108 (2005).
[43] H. C. Mayer and R. Krechetnikov, "Landau-Levich flow visualization: Revealing the flow topology responsible for the film thickening phenomena," Phys. Fluids **24**, 052103 (2012).
[44] P. A. Kralchevsky, V. N. Paunov, N. D. Denkov, and K. Nagayama, "Capillary image forces: I. Theory," J. Colloid Interface Sci. **167**, 47–65 (1994).
[45] A. Würger, "Curvature-induced capillary interaction of spherical particles at a liquid interface," Phys. Rev. E **74**, 041402 (2006).
[46] P. A. Kralchevsky, V. N. Paunov, and K. Nagayama, "Lateral capillary interaction between particles protruding from a spherical liquid layer," J. Fluid Mech. **299**, 105–132 (1993).
[47] D. Stamou, C. Duschl, and D. Johannsmann, "Long-range attraction between colloidal spheres at the air-water interface: The consequence of an irregular meniscus," Phys. Rev. E **62**, 5263–5272 (2000).
[48] K. D. Danov and P. A. Kralchevsky, "Capillary forces between particles at a liquid interface: General theoretical approach and interactions between capillary multipoles," Adv. Colloid Interface Sci. **154**, 91–103 (2010).
[49] D. L. Hu and J. W. M. Bush, "Meniscus-climbing insects," Nature (London) **437**, 733–736 (2005).
[50] M. Cavallaro, Jr., L. Botto, E. P. Lewandowski, M. Wang, and K. J. Stebe, "Curvature-driven capillary migration and assembly of rod-like particles," Proc. Natl. Acad. Sci. U.S.A. **108**, 20923–20928 (2011).
[51] In a static calculation, one of the parameters, either the contact angle, α, or angular positions of the contact line, θ_1 and θ_2, or the vertical position, h, needs to be specified. In the present analysis, we choose to fix α, but the procedure can easily be modified to vary α by fixing another parameter.
[52] The approach is also valid for floating particles with a change of sign of $\Delta\rho$.
[53] J. B. Keller, "Surface tension force on a partly submerged body," Phys. Fluids **10**, 3009–3010 (1998).
[54] For a single floating cylinder, $\theta_1 = \theta_2$. In this case, Princen[11] shows that the wetting angle approaches the value $(\pi - \alpha)$ in the limit $B \to 0$. This indeed corresponds to a flat interface at zero gravity and is the leading order solution in the present study.
[55] M. Berhanu and A. Kudrolli, "Heterogeneous structure of granular aggregates with capillary interactions," Phys. Rev. Lett. **105**, 098002 (2010).
[56] J. Lucassen, "Dynamic dilational properties of composite surfaces," Colloids Surf. **65**, 139–149 (1992).
[57] The force balance equation for each particle can be written as: $m\ddot{x} = F(x) - F_d(x, \dot{x}, \mu)$ where d is the separation distance, F is the capillary attraction force, and F_d is the drag force. In our preliminary experiments,[58] F and F_d were comparable in magnitude and the acceleration of the particles were negligible.
[58] Capillary attraction experiments were carried out with 0.78 mm glass spheres by varying the viscosity of the liquid. This was achieved by varying the mixture ratio of glycerol to distilled water. A drag coefficient, f_d, can be defined by normalizing the measured drag with the Stokes drag for a sphere. It was found that at small viscosities, $f_d > 1$ and at large viscosities, $f_d < 1$ and was found to be approximately constant.